Impact of Secondary Particle Size and Two-Layer Architectures on the High-Rate Performance of Thick Electrodes in Lithium-Ion Battery Pouch Cells

Marissa Wood[1,+,*], Jianlin Li[1,2], Zhijia Du,[1] Claus Daniel[1,2], Alison R. Dunlop[3], Bryant J. Polzin[3], Andrew N. Jansen[3], Gregory K. Krumdick[4], David L. Wood III[1,2,*]

[1]Electrification and Energy Infrastructure Division
Oak Ridge National Laboratory, Oak Ridge, TN 37831 USA

[2]Bredesen Center for Interdisciplinary Research and Graduate Education,
University of Tennessee, Knoxville, TN 37996, USA

[3]Chemical Sciences and Engineering Division; [4]Applied Materials Division
Argonne National Laboratory, Lemont, IL 60439, USA

*Corresponding Author
mwood@llnl.gov; wooddl@ornl.gov

Keywords: lithium-ion battery, electrode architecture, two-layer electrode, thick electrode, Li^+ mass transport limitations, pouch cell

[+]Currently at Lawrence Livermore National Laboratory

Lawrence Livermore National Laboratory is operated by Lawrence Livermore National Security, LLC, for the U.S. Department of Energy, National Nuclear Security Administration under Contract DE-AC52-07NA27344.

Abstract

Increasing lithium-ion battery gravimetric energy density to >300 Wh/kg, while simultaneously meeting a cost target of $80/kWh, is of paramount importance to increasing the driving range and affordability of EVs. One way to address this goal is to reduce inactive components by increasing electrode areal capacities, but conventional thick electrode designs typically perform poorly at high discharge rates due to Li^+ mass transport limitations. Here we compare the rate capability and cycle life of NMC 532/graphite pouch cells made with five different thick cathode and anode designs paired together in 25 combinations. We find that using different particle sizes to structure *both* the cathode and anode architectures in two-layer configurations results in a 2X capacity improvement over the worst-performing combination at high discharge rates (97 vs. 46 mAh/g at 2C). These different cathode/anode designs also translate to different cycle life performance, with many cells cycled at C/2 achieving ~80% capacity retention after 1000 cycles, and cells cycled at 2C showing different degrees of capacity fade. Overall, these results demonstrate that simple, scalable changes in electrode design can significantly improve the performance of thick electrodes for high energy density batteries.

1. Introduction

Battery electric vehicles (BEVs) are key to meeting new greenhouse gas regulations and reducing U.S. dependence on imported fossil fuels. However, they still have three critical limitations that are restricting widespread commercialization: high battery pack costs, limited driving range, and long recharge times. Currently consumers must pay a price premium for driving ranges in excess of ~250 miles. The state-of-the-art, commercial EV lithium-ion battery (LIB) gravimetric cell energy density is ~250-275 Wh/kg.[1,2] In order to simultaneously reach a 300-400-mile driving range and an affordable BEV cost of $80/kWh at the cell level (the ultimate target of the U.S. Department of Energy Vehicle Technologies Office), energy densities of at least 350-375 Wh/kg must be achieved.

There are several approaches to lowering the cell cost. One is to reduce the cost of active materials and the associated synthesis methods. Another is to reduce the number of inactive components in a cell (namely the current collector foils and separator), as both the Cu foil and the separator are in the top five most expensive subcomponents of an EV LIB pack.[3] This can simultaneously increase the energy density, since the current collector foils also add significantly to the weight of the cells. In order to decrease these inactive components, each electrode must provide a higher individual capacity so that fewer layers are required to achieve the same overall cell capacity. This can be accomplished by either raising the specific capacity of the active materials (such as by increasing the Ni content of the cathode,[4] adding Si to the graphite anode,[5] or replacing graphite with Li metal[6]), or alternatively by substantially increasing the areal capacity (thickness) of each electrode.[7]

The latter is a more straightforward approach, but high areal capacities lead to poor high-power performance (i.e. low specific capacity at high discharge rates) due to Li^+ mass transport limitations in the liquid electrolyte phase.[8–10] The ultimate target cathode areal capacity of the DOE Battery Manufacturing R&D Facility (BMF) at ORNL is ~8 mAh/cm^2. Going much above this value (i.e. ~180 µm thick) leads to a point of diminishing returns in volumetric energy density, as the porosity of the calendered electrodes becomes the dominating factor.[11] Performance

limitations due to poor Li^+ mass transport have been observed in several thick homogeneous electrode studies. For example, one study reported "semi-solid" electrodes as thick as 450 µm or higher (i.e. ≥ 13 mAh/cm^2), but they suffer from severe mass transport limitations and volumetric energy density penalties at even modest discharge rates (> C/2) and cannot currently fulfil the high discharge rate and fast charging needs of BEVs.[12] Likewise, another found substantial electrode Li^+ diffusion resistance for thick 3.6 mAh/cm^2 $LiNi_{0.33}Mn_{0.33}Co_{0.33}O_2$ (NMC 333) electrodes between discharge rates of 1 and 5C,[13] and Singh et al. observed a 37% performance drop for a thick 320 µm (43 mg NMC/cm^2) NMC 333 electrode compared to a 70 µm (10 mg/cm^2) electrode, even at a low discharge rate (C/2).[14] They followed this initial work with an electrode thickness and cell volumetric energy optimization study,[15] finding that the best performing areal capacity was 6.5 mAh/cm^2 (155 µm), which maintained most of its rated capacity at C/2; however, this was the maximum discharge rate evaluated, which is still quite low. In addition, Gallagher et al. examined thick, homogeneous electrodes in $LiNi_{0.6}Mn_{0.2}Co_{0.2}O_2$ (NMC 622)/graphite full cells within a cathode areal capacity range of 2.2-6.6 mAh/cm^2 (48-154 µm) and found that there was a drop of almost 50% in the high-rate specific capacity at 1-2C discharge rates for the 6.6 mAh/cm^2 electrode.[16] These studies highlight the need for more advanced thick electrode designs capable of achieving high capacities at high power densities.

There have been several modeling studies exploring the effectiveness of porosity grading and particle size variation as strategies for improving mass transport in thick electrodes, although the conclusions have been mixed. Most of the studies show that these measures are effective approaches to increase high-power performance and energy density simultaneously. For example, Golmon et al. showed that both particle size and porosity grading resulted in improved performance at 2 mA/cm^2 current density.[17,18] Although, this is still a low value with respect to cell power density, these studies predicted a 61% cell specific capacity improvement at these operating conditions when the pore size and particle size distributions were optimized. Likewise, Liu et al. showed that porosity grading was effective for $LiNi_{0.5}Mn_{1.5}O_4$ (LNMO)/graphite cells in terms of gravimetric and volumetric energy density and capacity

fade,[19] and Qi et al. found that a higher cathode porosity at the separator and a lower porosity at the current collector was an effective strategy for improving cell performance.[20]

Conversely, two modeling studies showed that porosity grading was not an effective strategy for increasing either gravimetric or volumetric energy density. Dai and Srinivasan found no difference in mathematical simulations of a $LiMn_2O_4$/graphite cell chemistry between optimized homogenous electrodes and ones with graded porosity.[21] However, one major limitation of this study is that it focused on discharge rates ≤ 1C, i.e. rates where the power densities and associated liquid-phase Li^+ mass transport limitations are low. Also, they only examined a narrow range of cathode porosities (between 0.15 and 0.28). Similarly, Du et al. concluded that porosity grading in different ways over a wide range of porosities (0.15 to 0.45) yields only a minimal increase in volumetric energy density (from 580 Wh/L to 590 Wh/L).[11] However, they also found that varying the particle size had a large effect in a homogenous electrode. It should be noted that the latter finding, in effect, is another method of varying pore size distribution within a homogeneous electrode. The simulations considered C/5, C/2, and 2C discharge rates, but one major limitation of this study is that it did not consider the effect of simultaneously varying the anode porosity. Other modeling studies have also shown improved high-rate performance by implementing more ordered architectures with decreased tortuosity. For example, Mai and coworkers found that an array of vertical channels can be optimized together with electrode porosity to enable energy density improvements of 30% when cells are fast charged at 6C,[22] and Cobb et al. evaluated different cathode designs with varied open channel dimensions and porosity that yielded high-rate capacity improvements at the pouch cell level.[23]

Similarly, several experimental studies have also demonstrated improvements in high-rate charge and discharge capacity by fabricating electrode architectures that decrease tortuosity and improve Li^+ transport.[24,25] For example, Sander et al. used magnetic templating to create vertical channels in thick $LiCoO_2$ (LCO) cathodes with sacrificial functionalized nylon rods, demonstrating a 3X capacity improvement over the non-structured cathode at a 2C discharge rate.[26] Likewise, Billaud and coworkers employed a magnetic field to align functionalized

graphite flakes in a vertical orientation to create less tortuous Li^+ diffusion paths, showing a 3X improvement in charge capacity at 1C compared to the non-architected anodes,[27] and Ashby et al. improved the performance of $LiFePO_4$ (LFP) cathodes by fabricating arrays of vertical pillars with optimized dimensions in an ionogel electrolyte.[28,29] In addition, several studies have used freeze-casting to create different architectures. Behr et al. showed high-rate capacity improvements in freeze-cast $LiNi_{0.8}Co_{0.15}Al_{0.05}O_2$ (NCA) cathodes with ordered porous channels,[30] and Huang et al. explored different porosity gradients in thick (900 μm) freeze-cast $LiFePO_4$ (LFP) cathodes, finding that the cathode with lower porosity near the separator and higher porosity near the current collector showed the best performance at high discharge rates.[31]

Several groups have also used laser patterning to create 3D architectures. Chen et al. recently demonstrated that a graphite anode with an array of laser-drilled vertical channels can be fast charged at rates > 4C with significantly improved capacity retention compared to unpatterned electrodes (> 97% vs 69%, respectively),[32] and Smyrek and coworkers used laser ablation to create micro-pillar arrays in an NMC 333 cathode that enabled improved cycling at a discharge rate of 2C.[33,34] Various extrusion processes have also been used to create different electrode architectures. Bae and coworkers used successive co-extrusion steps to fabricate an array of vertical channels that improved the 2C discharge capacity by ~3X,[35] and Sun et al. used 3D printing to fabricate thick $Li_4Ti_5O_{12}$ (LTO) lattices with high areal capacity (4.74 mAh/cm^2) that maintained 80% capacity at 5C charge/discharge rates.[36] Other 3D printed batteries have also performed well.[37]

However, these approaches often require complicated templating and patterning methods that necessitate additional time, cost, and materials for fabrication and can be difficult to scale. There have been far fewer reports examining the effect of more scalable methods, such as varying the particle size and configuration, although there have been a few. For example, Xue and coworkers found that employing smaller LNMO particles improved the rate capability in coin cells,[38] and others have demonstrated the benefits of two-layer electrode designs.

Whitacre et al.[39] layered different cathode materials to take advantage of the high-rate capability of LFP and the high specific energy of $Li[Li_{0.17}Mn_{0.58}Ni_{0.25}]O_2$, while several other groups fabricated layered electrodes containing different amounts of binder[40,41] or conductive additives[42] for improved rate performance. However, most of these two-layer designs varied the electrode *composition*, with very few reports varying the active material *particle size*. Chen et al.[43] investigated the use of graphite materials with different planar sizes, and Huang et al.[44] demonstrated improved rate performance with large TiO_2 particles next to the current collector and small TiO_2 particles near the separator, but the effect of particle size in two-layer designs has yet to be fully explored. Overall, these studies with more scalable design approaches investigated a limited number of electrode designs, were mostly conducted in coin cells rather than pouch cells, and examined designs in only one half of the cell (either the cathode or anode).

In this work, we explored the influence of active material particle size and particle configuration on the high-rate capability and long-term cycle life of single-layer pouch cells made with thick electrodes (3.7 mAh/cm^2 cathodes and 4.8 mAh/cm^2 anodes). A matrix of 5 different anodes and 5 different cathodes were prepared using two particle sizes (2 homogeneous single-layer baseline electrodes, 1 single-layer electrode with mixed particle size, and 2 two-layer electrodes containing both particle sizes), and the pore size distributions in the electrodes were characterized by mercury porosimetry. Each cathode was paired with each anode for a total of 25 different combinations. We found that simple changes in particle size and configuration can significantly improve the high-rate discharge capacity. Changing the cathode active material particle size from 12 µm to 6 µm improved the 2C discharge capacity by 1.8X, but the best performing combination was determined to be a two-layer cathode with large particles near the current collector and small particles near the separator paired with a two-layer anode with small particles near the current collector and large particles near the separator, which showed a 2X capacity improvement over the single-layer baseline cell at a 2C discharge rate. Cells made with different electrodes designs also showed significant differences in capacity retention after long-term cycling at a discharge rate of C/2, but several cathode/anode combinations achieved

> 120 mAh/g (> 80% retention) after 1000 cycles. Although increasing the cycling rate to 2C caused significant capacity fade for all cells, there was still variation in the performance based on the electrode combination used, and the electrode designs could be further tailored to improve this high-rate cycle life performance. While in general changes to the cathode made a bigger difference than changes to the anode, these results demonstrate that the combination of *both* electrodes is important for optimizing performance.

2. Experimental

2.1 Electrode Fabrication & Pouch Cell Assembly

Cathodes and anodes were fabricated according to the five designs shown in Figure 1. Cathode dispersions were prepared by mixing 90 wt% $LiNi_{0.5}Mn_{0.3}Co_{0.2}0_2$ (NMC 532; Toda America, Inc.), 5 wt% polyvinylidene difluoride (PVDF, Solvay 5130), and 5 wt% carbon black (Denka Li-100) in N-methylpyrrolidone (NMP, Sigma-Aldrich). Anode dispersions were prepared by mixing 91.83 wt% graphite (Superior Graphite; 1520P for large particle or 1506T for small particle), 6 wt% PVDF (Kureha 9300), 0.17 wt% oxalic acid (to help with adhesion to the current collector), and 2 wt% carbon black (Imerys C-NERGY C45) in NMP. The small and large NMC 532 cathode particle sizes (d_{50}) were 6 µm and 12 µm, respectively, and the small and large anode graphite particle sizes (d_{50}) were 9 µm and 18 µm, respectively.

The mixed particle size electrodes (#2 in Figure 1) were prepared according to these same formulations, but with a 50/50 wt% ratio of the two active material particle sizes. Electrodes were coated onto either aluminum or copper foil (MTI Corporation) using a pilot-scale slot-die coater (Frontier Industrial Technology) at a total loading of ~25 mg/cm^2 (3.7 mAh/cm^2) for the cathodes and ~15 mg/cm^2 (4.8 mAh/cm^2) for the anodes. The two-layer coatings (#3 and #4 in Figure 1) were made by coating one layer first and allowing it to dry before coating the second layer on top. All electrodes were calendered to ~35% porosity and dried at 115 °C in a vacuum oven overnight (secondary drying) before cell assembly.

Single-layer pouch cells were assembled in a dry room (≤0.3% relative humidity) using Celgard 2325 as the separator and 1.2M $LiPF_6$ in 3:7 wt% ethylene carbonate/ethyl methyl carbonate (Soulbrain MI) as the electrolyte. The cathode and anode dimensions were 8.4 cm L x 5.6 cm W and 8.6 cm L x 5.8 cm W, respectively, giving a total cell capacity of ~174 mAh. Each cathode and anode design were paired together to give 25 total combinations. Cells were made in triplicate, and a stack pressure of 35 kPa (5 psi) was applied to all cells before cycling.

2.2 Electrochemical Testing

Pouch cells were cycled between 2.5 V and 4.2 V following a CCCV protocol, in which they were charged to 4.2 V and held at that voltage until the current dropped to C/20 before discharging. All cells were first charged at C/10 for 15 min, and then allowed to rest for 6 h before cycling to facilitate electrolyte wetting. They were then subjected to formation cycling at C/20 (charge and discharge) for 4 cycles before further rate performance and cycle life testing.

Rate performance was evaluated by keeping the charge rate constant at C/5 and varying the discharge rate from C/10 to 10C. Three cycles were run at each C rate, and the results were averaged together across all three cells for each cathode/anode combination. Long-term cycle life testing was performed at two different discharge rates (C/2 and 2C) for 1000 cycles each. The charge rate was kept constant at C/2 in both cases, and hybrid pulse power characterization (HPPC) was performed after every 100 cycles. For each HPPC test, cells were first charged to 4.2V at C/3, held at 4.2V until the current dropped to C/20, then allowed to rest for 1 h. Then the following protocol was repeated 9 times: discharge 10% of the capacity at C/3, rest for 1 h, discharge at 2C for 10 s, rest for 40 s, charge at 1.5C for 10 s, rest for 40 s. The results from all three cells made with each cathode/anode combination were averaged together. All data was recorded at 30 °C in a temperature chamber (ESPEC) using a Maccor battery cycler (Series 4000).

2.3 Electrode Characterization

Cross-section SEM images were acquired using a JEOL JSM-6610LV instrument (Argonne National Laboratory) and a Zeiss Merlin instrument (Oak Ridge National Laboratory). Mercury

porosimetry was performed by Porous Materials, Inc. (Ithaca, New York) and gives specific pore volume as a function of mercury intrusion pressure. Pore diameter at a given pressure was estimated using a cylindrical pore shape approximation.

3. Results and Discussion

3.1 Rate Performance of Single-Layer Electrodes with Different Particle Sizes

The effect of active material particle *size* and *configuration* on the high-rate performance of single-layer pouch cells made with thick electrodes (~3.7 mAh/cm^2 cathodes and 4.8 mAh/cm^2 anodes) was investigated by preparing five different anodes and five different cathodes according to the designs shown in Figure 1. The first two are single-layer baseline electrodes with small and large active material particle sizes (denoted as samples "1" and "5"), the third one is a single-layer electrode with the small and large particles mixed together (50/50 wt%; denoted as sample "2"), and the last two are two-layer electrodes in two different configurations: one with a layer of large particles on the bottom near the current collector and a layer of small particles on the top near the separator (denoted as sample "3") and one with

the opposite configuration (denoted as sample "4"). Hereafter, each electrode will be referred to by either "C" for cathode or "A" for anode followed by these sample labels for simplicity. All electrodes were slot-die coated with a total loading of ~25 mg/cm^2 for the cathodes and ~15 mg/cm^2 for the anodes. The different electrode structures were confirmed by cross-sectional SEM images (Figure 2), which clearly show the difference between the small and large particle sizes, as well as the distinct, symmetrical layers of electrodes 3 and 4.

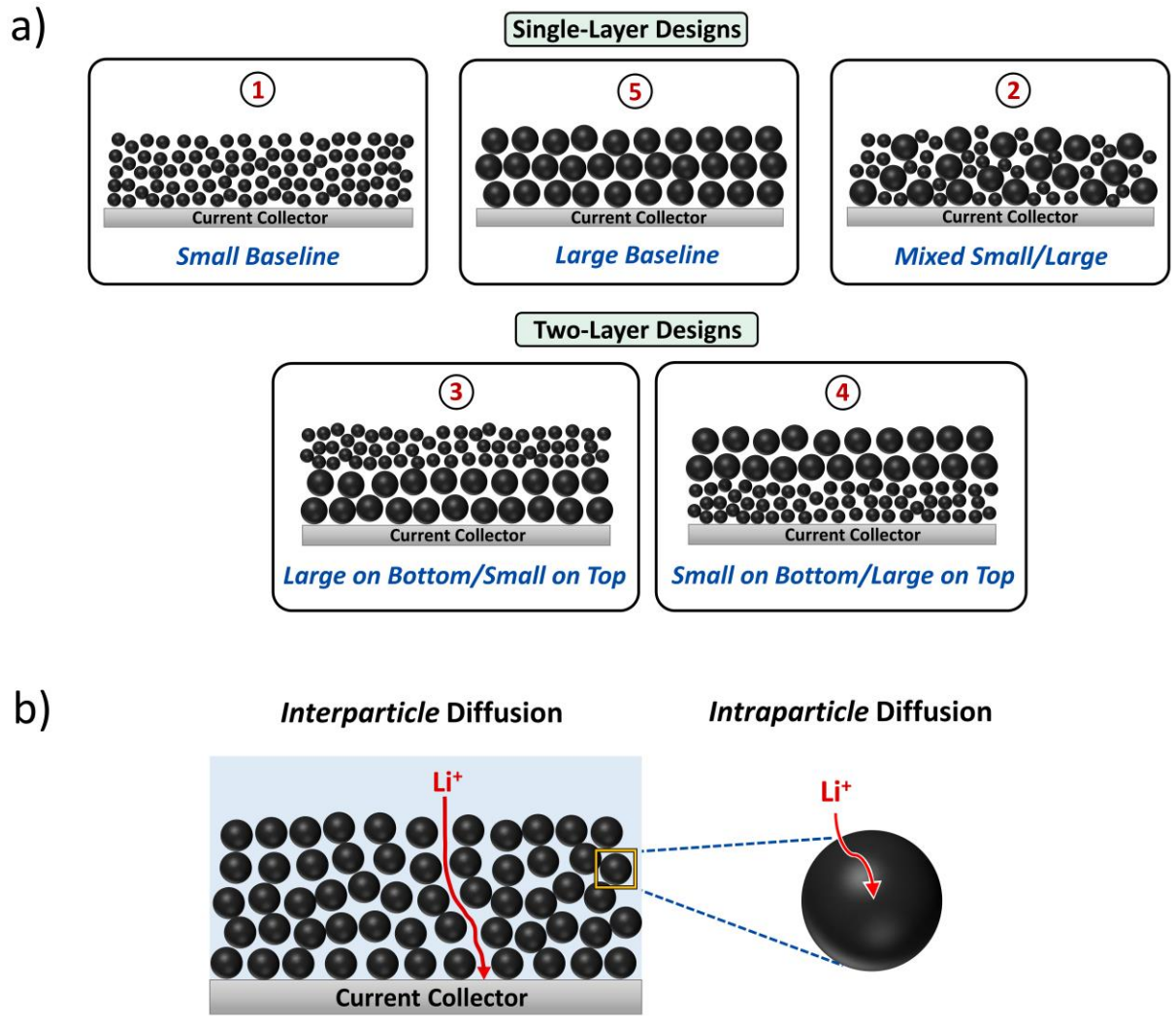

Figure 1. a) Thick electrode designs with different active material particle sizes and configurations. b) Schematic of *interparticle* and *intraparticle* diffusion pathways in a thick electrode.

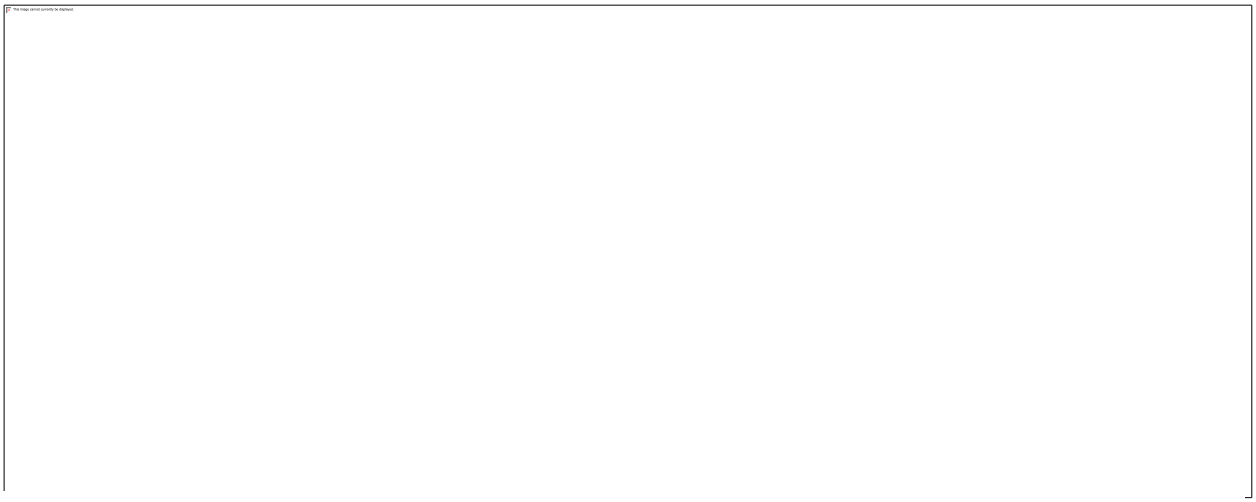

Figure 2. SEM cross-sections of cathodes (top row) and anodes (bottom row) prepared according to the designs in Figure 1. All electrodes were calendered to ~35% porosity.

The two different active material particle sizes have distinct advantages and disadvantages (illustrated in Figure 1b). Smaller particles provide a higher surface-area-to-volume ratio, which creates shorter *intraparticle* diffusion pathways and facilitates more complete utilization of each particle, but their small size results in more tortuous *interparticle* diffusion pathways when packed, which can limit Li^+ diffusion. Conversely, larger particles have a lower surface-area-to-volume ratio, which creates longer *intraparticle* diffusion pathways, but their larger size results in less tortuous *interparticle* diffusion pathways when packed, which should facilitate Li^+ diffusion. The average diameters of the small particles used in this work were ~2 times smaller than the average diameters of the large particles (d_{50} = 6 µm and 12 µm for the cathode; d_{50} = 9 µm and 18 µm for the anode, which is a significant enough variation to generate observable differences.

Single-layer pouch cells were assembled with each cathode and anode combination (25 total combinations made in triplicate) and subjected to rate capability testing at different discharge rates. To isolate the effect of particle size, only the results for cells made with *single-layer* electrodes are compared in Figure 3. There was very little performance difference for any of the cells at discharge rates below 1C, where liquid-phase Li^+ mass-transport is not limiting. Although the performance began to diverge at 1C, the greatest differences occurred at 2C. For example, changing the cathode particle size from large to small while keeping the same large particle anode (C1/A5 and C5/A5; solid blue and green lines) dramatically improved the capacity at 2C, increasing it from 50 to 91 mAh/g (30% to 55% of the rated capacity). This difference is likely due to the higher active material surface area provided by the small particles, which makes it easier for Li^+ to diffuse through the entirety of each particle and

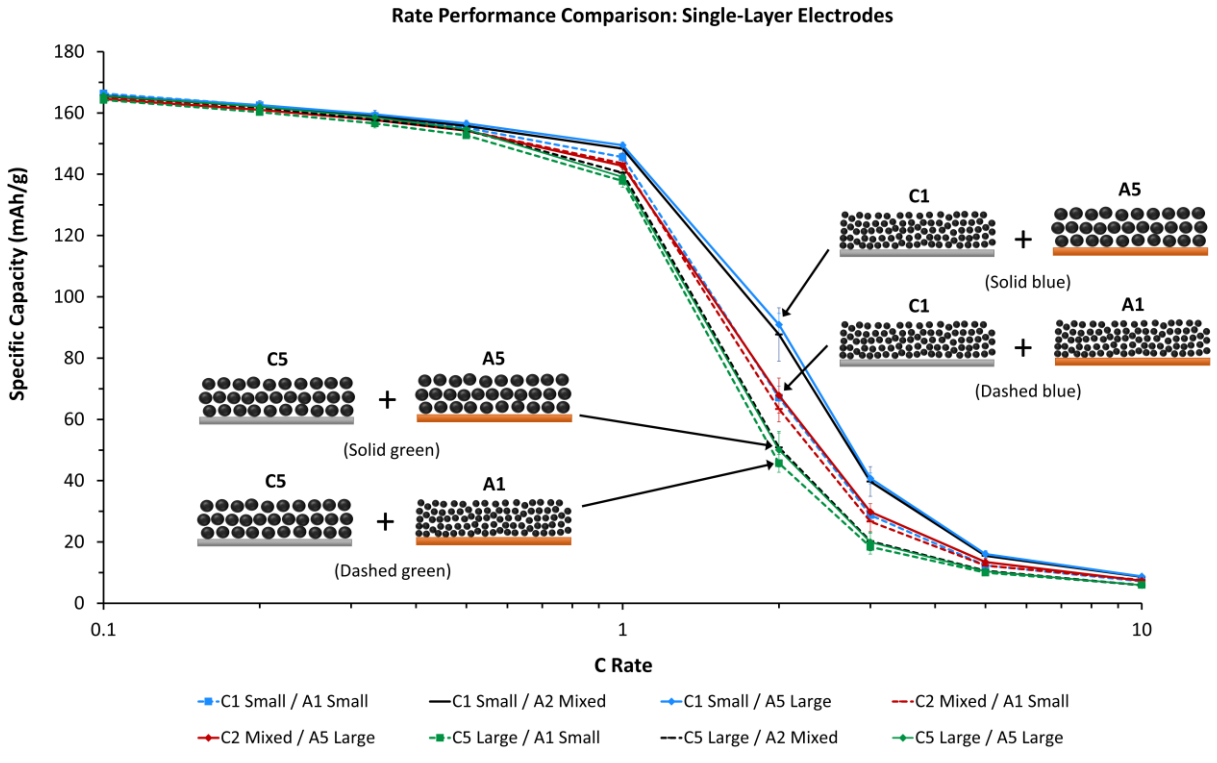

Figure 3. Rate performance comparison for single-layer pouch cells assembled with different *single-layer* cathode/anode combinations. The charge rate was held constant at C/5 while the discharge rate was varied. Each point is an average of 3 cells, and error bars represent the standard deviation of these 3 cells.

increases the percentage of active material utilized. These results agree nicely with modeling predictions from Du et al., which showed that smaller active material cathode particles enable higher energy densities at fast cycling rates,[45] and experimental work from Xue et al. demonstrating better rate capability with smaller LNMO particles.[38]

Interestingly, the choice of paired anode also made a difference. When these same two cathodes were compared in cells made with the *small* particle anode instead (C1/A1 and C5/A1; dashed blue and green lines), the difference at 2C was not as substantial, only showing a capacity increase from 46 to 67 mAh/g (28% to 40% of the rated capacity). In other words, some of the beneficial effects of the small particle cathode are dampened by the limitations of the small particle anode. Although small particles improve the cathode performance, they may be detrimental to the anode performance because the increased surface area must be passivated by the solid electrolyte interphase (SEI) layer. Post-processing of the graphite surface plays a role in SEI layer chemistry and performance;[46,47] however, the SEI layer is somewhat resistive and may impede Li^+ diffusion at faster discharge rates. In addition, lithium intercalation in graphite particles occurs at the edge planes, making it orientation specific.[46,48] It is possible that these edge planes are more accessible in the large particle anode due to the increased interstitial space between particles, leading to faster Li^+ diffusion at high rates.

To isolate the effect of particle size for just the anode, the performance of cells made with the *same* small particle cathode but two *different* particle size anodes (C1/A1 and C1/A5; dashed blue and solid blue lines) was also compared. The cell made with the *large* particle anode performed significantly better at 2C (91 mAh/g; 55% of rated capacity) compared to the cell made with the *small* particle anode (67 mAh/g; 40% of rated capacity), again confirming that large particles are beneficial for the anode. On the other hand, when these same two anodes were paired with the *large* particle cathode instead (C5/A1 and C5/A5; dashed green and solid green lines), there was very little difference in the capacity at 2C (46 vs 50 mAh/g; 28% vs 30% of rated capacity), likely because the performance of the large particle cathode itself was poor, so changing the anode had little effect.

Since both particle sizes have certain hypothetical advantages, electrodes were also prepared with the large and small particles mixed together in a 50/50 wt% ratio. The capacity retention of the *mixed* cathode (C2 red solid and dashed lines) at 2C was between the small and large cathode results, giving from 63 to 68 mAh/g (38% and 41% of rated capacity) when paired with the small (A1) and large (A5) particle anodes, respectively. In this case, the choice of anode again had very little effect. This observation may be explained by the fact that the mixed cathode performance was worse than the small particle cathode (C1) performance, and the anode appears to only make a significant performance difference if the cathode performance is also good. This explanation is further supported by the results for the mixed particle *anode* (A2), which exhibited significantly higher capacity at 2C (88 mAh/g; 53% of rated capacity) when paired with the *small* particle cathode (C1; solid black line) compared to the *large* particle cathode (C5; dashed black line; 51 mAh/g; 31% of rated capacity), suggesting that the choice of cathode makes a more significant difference than the choice of anode.

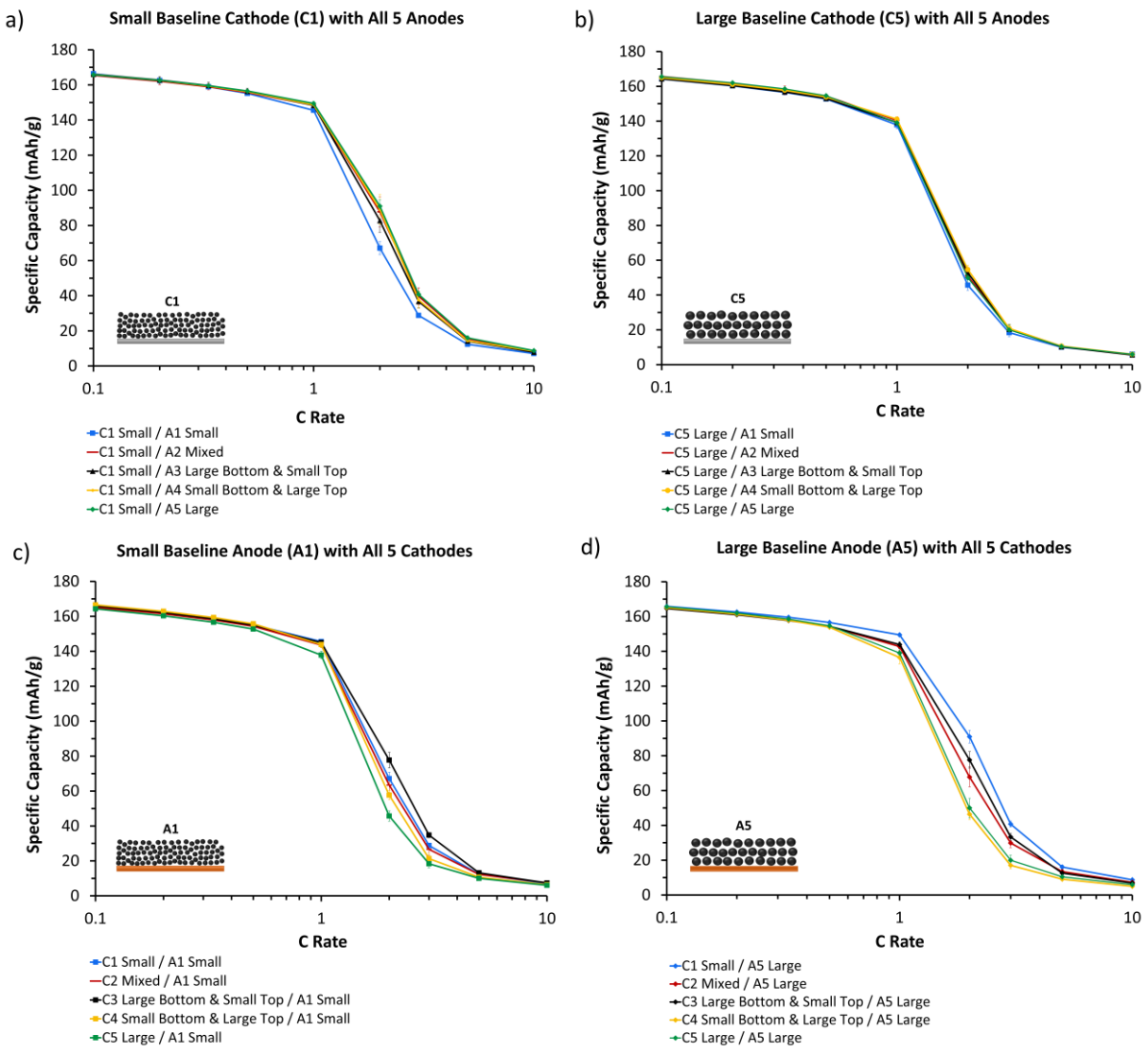

Figure 4. Rate performance of each baseline electrode paired with all five matching electrode designs. a) Small baseline cathode (C1); b) Large baseline cathode (C5); c) Small baseline anode (A1); d) Large baseline anode (A5); The charge rate was held constant at C/5 while the discharge rate was varied. Each point is an average of 3 cells, and error bars represent the standard deviation of these 3 cells.

The importance of cathode particle size is further confirmed by examining the performance of each baseline cathode (C1 and C5) paired with all five anodes, and each baseline anode (A1 and A5) paired with all five cathodes (Figure 4). The *overall* capacity was much higher at 2C for the small particle cathode (C1) set (Figure 4a) than the large particle cathode (C5) set (Figure 4b),

matching the observation from Figure 3. However, the *variation* within each of these sets is low, confirming that changing the anode has only a small effect on the overall rate performance. For example, the capacities of the small particle (C1) cells ranged from only 83 to 91 mAh/g at 2C (50% to 55% of rated capacity), with the exception of the C1/A1 pairing (which was significantly lower than the others at 67 mAh/g), while the capacities of the large particle (C5) cells ranged from only 46 to 55 mAh/g (28% to 33% of rated capacity). Conversely, both the small particle anode (A1) and large particle anode (A5) sets (Figure 4c and d, respectively) showed much more variation with different *cathode* pairings, with the A1 cells reaching between 46 and 78 mAh/g at 2C (28% and 47% of rated capacity), and the A5 cells reaching between 46 and 91 mAh/g at 2C (28% and 55% of rated capacity). Overall, the single-layer electrode results demonstrate that the choice of particle size is critical for both the anode and cathode and can lead to substantially different electrochemical performance. However, changing the *cathode* particle size produces the largest difference.

3.2 Rate Performance of Structured Two-Layer Electrodes with Different Particle Configurations

As discussed in Section 1, other researchers have suggested that creating different pore size distributions in the electrodes may help improve the rate performance (or hinder it if not designed properly). Therefore, two-layer electrodes were also prepared with two different configurations: a large particle layer on the bottom near the current collector and a small particle layer on top near the separator, and the opposite with a small particle layer on the bottom near the current collector and a large particle layer on top near the separator. Figure 5a shows the rate performance of all cells made with only these two-layer *cathodes* (paired with each of the five anodes). There was a clear difference between the two configurations, with all of the cells containing two-layer cathodes with the large particles near the current collector (C3, blue lines) performing much better (78 to 97 mAh/g at 2C; 47% to 59% of rated capacity) than those with the small particles near the current collector (C4, red lines; 46 to 68 mAh/g at 2C; 28% to 41% of rated capacity). Some variation was still observed within each group due to anode differences.

The C3 configuration is likely better than the C4 configuration because having a layer of small particles near the separator provides a high active material surface area that facilitates faster Li^+ intercalation throughout each of the cathode particles. However, mass transport becomes more limited towards the current collector. Therefore, having a layer of large particles near the

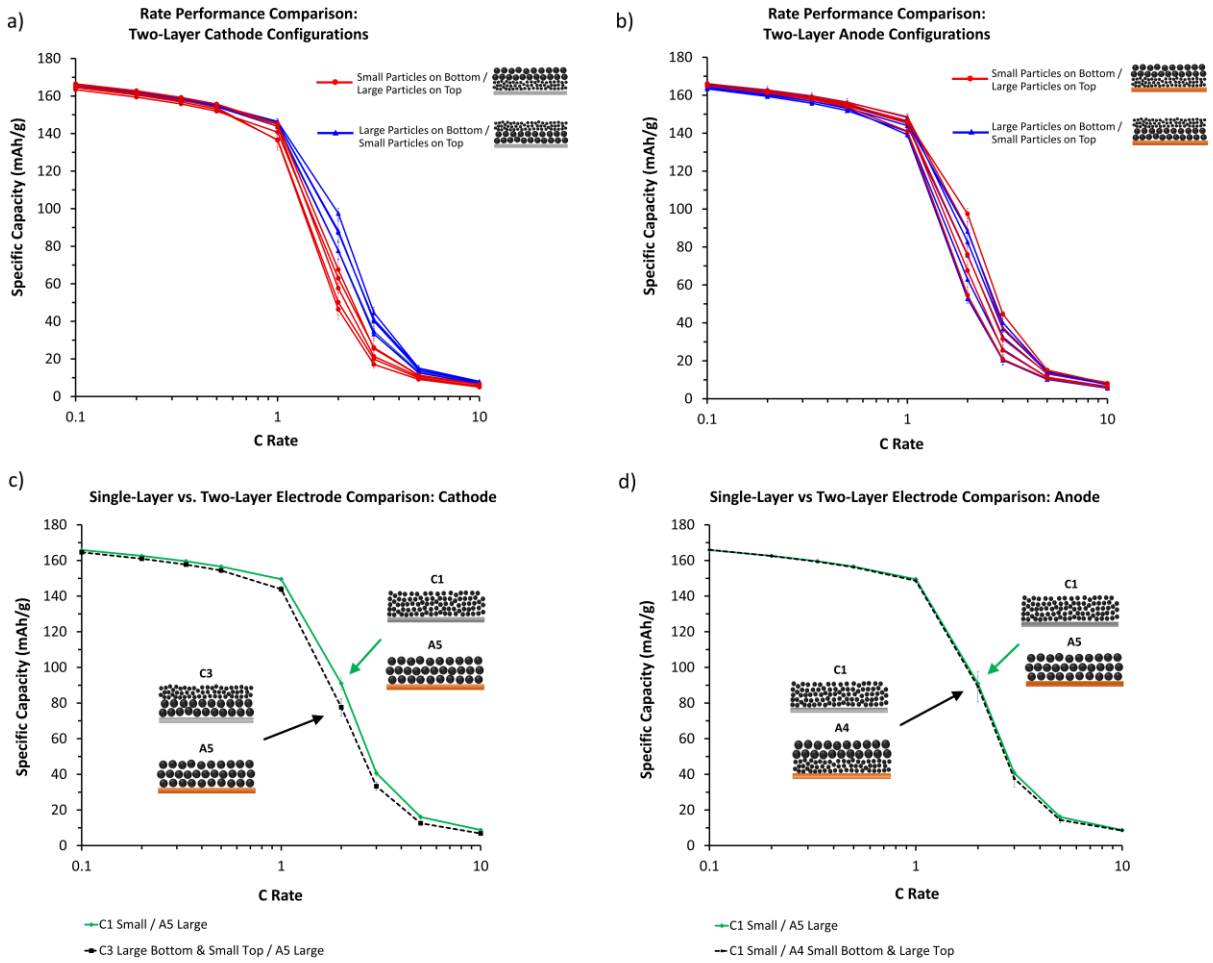

Figure 5. Comparison of single-layer pouch cells made with single-layer and two-layer electrodes. a-b) Rate performance of cells made with two-layer cathodes (a) and two-layer anodes (b) with different configurations: large particles on the bottom near the current collector with small particles on top (blue) and small particles on the bottom near the current collector with large particles on top (red). c-d) Rate performance of cells made with single-layer and two-layer cathodes (c) and single-layer and two-layer anodes (d) paired with matching baseline electrodes. In all cases, the charge rate was held constant at C/5 while the discharge rate was varied. Each point is an average of 3 cells, and error bars represent the standard deviation of these 3 cells.

current collector is likely beneficial because, although the large particles have a lower surface

area, their packing generates less tortuous pathways between the particles, providing enhanced *interparticle* diffusion to reach the entirety of the electrode. This could help alleviate what would otherwise be a sharp Li^+ concentration gradient. This explanation is supported by previous reports of performance improvement for electrode designs with larger particles or lower tortuosity near the current collector and smaller particles or higher tortuosity near the separator.[31,44] Conversely, for the reverse configuration, the better *interparticle* diffusion pathways provided by the large particle layer are likely not as advantageous near the separator, since mass transport is less of an issue at the surface of the electrode. Therefore, this large particle layer likely hinders *intraparticle* Li^+ transport due to its lower surface area. As the Li^+ ions travel further to the small particle layer near the current collector, the enhanced *intraparticle* Li^+ transport resulting from the higher surface area small particles is likely less beneficial as *interparticle* diffusion becomes increasingly limited.

Figure 5b shows all of the cells made with two-layer *anodes* and each of the five cathodes. Unlike the distinct trend observed for the cathodes, the particle size configuration in the anode did not affect the rate performance in a discernible way, with no clear difference between the results from cells containing anodes with large particles near the current collector (A3, blue lines) and those containing anodes with small particles near the current collector (A4, red lines). This again is likely due to the fact that the *cathode* performance dominates the overall cell performance, making it harder to detect a trend with the anodes.

A comparison of all 25 electrode combinations clearly illustrates that the performance at high discharge rates can be substantially improved by selecting the appropriate electrode *particle size* and *configuration* (Figure 6). In fact, this plot shows a two-fold increase in the capacity at 2C, with the worst-performing cells (C5 single-layer large particle cathode paired with A1 single-layer small particle anode and C4 two-layer cathode with small particles near current collector paired with A5 single-layer large particle anode) achieving only 46 mAh/g at 2C (28% of rated capacity), and the best-performing cell (C3 two-layer cathode with large particles near current collector paired with A4 two-layer anode with small particles near current collector) reaching

97 mAh/g (59% of rated capacity). The plot was color coded by cathode to facilitate easy comparison, and it revealed a clear correlation between cathode composition and cell performance. Although the results for each cathode overlapped somewhat, in general they followed a particular order at 2C. Cells made with the small particle cathode (C1; blue lines) or the two-layer cathode with large particles near the current collector (C3; black lines) clearly performed better than all the others, with overlapping capacities ranging from 67 to 97 mAh/g (40% to 59% of rated capacity). Cells made with the mixed cathode (C2; red lines) showed mid-

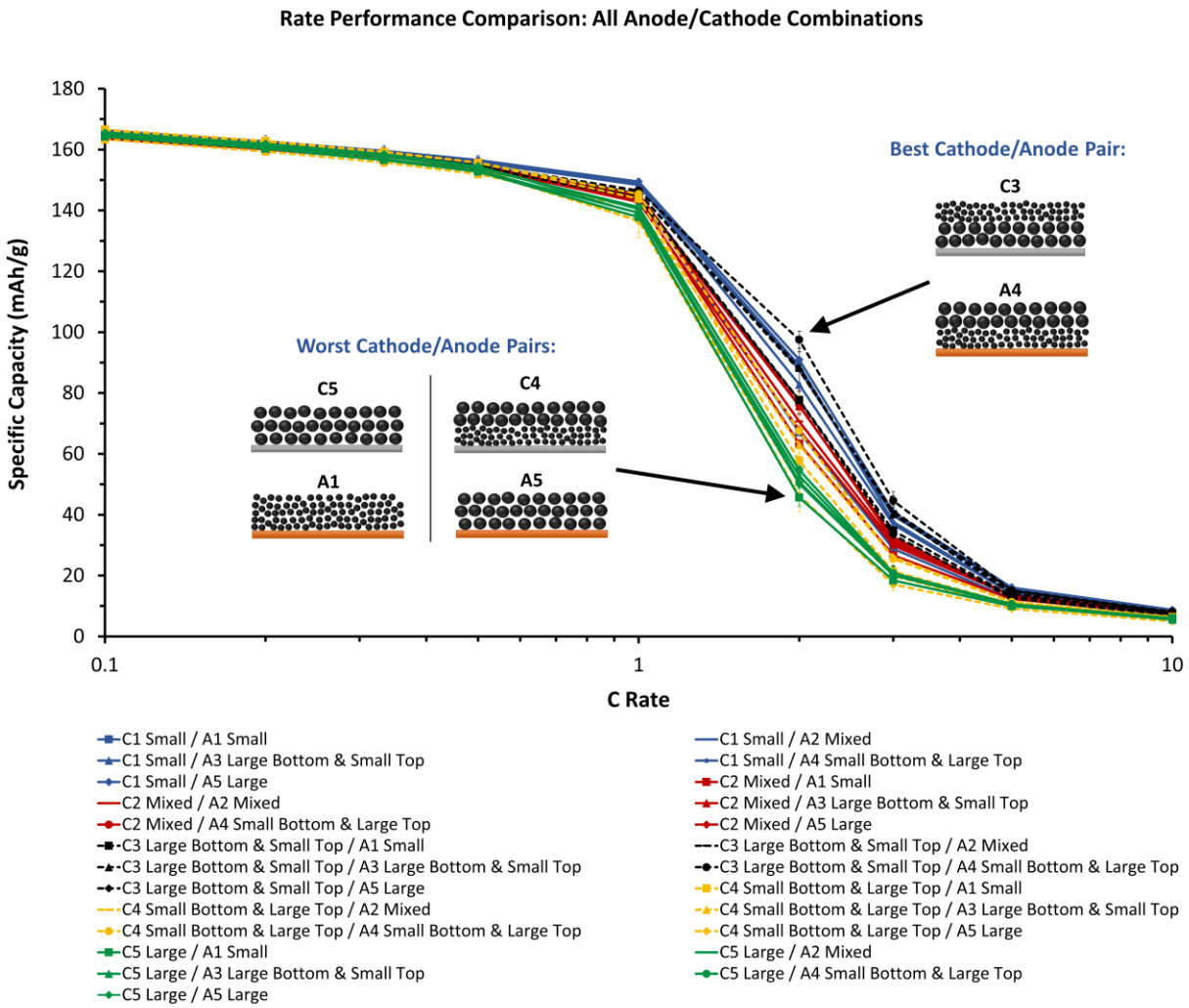

Figure 6. Rate performance comparison for single-layer pouch cells assembled with all twenty-five cathode/anode design combinations. Cells are color coded according to cathode: C1 blue, C2 red, C3 black, C4 yellow, and C5 green. The dashed lines represent cells made with two-layer cathodes. The charge rate was held constant at C/5 while the discharge rate was varied. Each point is an average of 3 cells, and error bars represent the standard deviation of these 3 cells.

range performance, reaching 63 to 76 mAh/g (38% to 46% of rated capacity), while those made with two-layer cathodes with small particles near the current collector (C4; yellow lines) showed poor performance, achieving only 46 to 68 mAh/g (28% to 41% of rated capacity). Finally, cells made with single-layer large particle cathodes (C5 green) displayed the worst performance, reaching only 46 to 55 mAh/g (28% to 33% of rated capacity). In summary, the results were: C1 (blue) ~C3 (black) > C2 (red) > C4 (yellow) > C5 (green).

These results demonstrate that the cathode composition substantially influences the high-rate performance and again confirm that the cell performance is dominated by the cathode. In particular, they suggest that increasing the active material surface area (by decreasing the particle size; C1) makes the biggest difference in performance, but a reduction in this surface area can be roughly compensated by providing less tortuous diffusion paths near the current collector (C3). This confirms that both particle *size* and *configuration* matter, a conclusion that is further supported by comparing the performance of the mixed particle cathode (C2) and the two-layer cathodes (C3 and C4), which all contained 50 wt% small particles and 50 wt% large particles, but arranged in different *configurations*. Mixing the two particle sizes together in a random orientation (C2; red lines) offered some improvement in surface area and tortuosity that resulted in higher capacity compared to the large particle cathode (C5; green lines), but mixing these two particle sizes together in an *ordered* manner, with large particles on the bottom providing decreased tortuosity (C3; black lines), resulted in a much larger performance enhancement. Conversely, maintaining the ordered design, but in the opposite orientation, with small particles near the current collector creating *increased* tortuosity (C4; yellow lines), resulted in the worst performance of the three.

While the anodes did not show a clear trend like the cathodes, the rate performance results also show that the cathode and anode performance cannot be completely decoupled from one another, and both are integral in determining the overall cell performance. This connection is illustrated in the following series of comparisons. First, the performance of the best single-layer and two-layer electrodes were directly compared (Figure 5c and d). When the same

baseline large particle anode (A5) was used, changing the cathode from a *single-layer* small particle electrode (C1; solid green line) to a *two-layer* electrode with large particles near the current collector (C3; dashed black line) actually *decreased* the overall performance from 91 to 78 mAh/g at 2C (55% to 47% of rated capacity; Figure 5c). Similarly, when the same small particle baseline cathode was used (C1), changing the anode from a *single-layer* large particle electrode (A5; solid green line) to a *two-layer* electrode with small particles near the current collector (A4; dashed black line) did not change the performance at 2C (91 to 89 mAh/g; 55% to 54% of rated capacity; Figure 5d). However, *combining* the best two-layer cathode with the best two-layer anode (C3/A4) produced the cell with the top performance out of all twenty-five combinations (97 mAh/g at 2C; 59% of rated capacity), demonstrating the importance of the cathode and anode *pairing.* This may be due to simultaneous minimization of anode and cathode liquid-phase Li^+ concentration gradients. In other words, Li^+ diffusion within each electrode may be limited to different degrees depending on which electrode it is paired with. This finding is supported by modeling work by Mai et al., which showed improved high-charge-rate energy density when *both* the cathode and anode were structured with low-tortuosity vertical channels.[22] However, it is important to note that our results show the C3/A4 capacity was only slightly higher than the best-performing *single-layer* combination (C1/A5, 91 mAh/g; 55% of initial capacity), indicating that the active material particles in the bottom layer of the two-layer electrodes are likely not being fully utilized. Both the best (C3/A4) and worst (C5/A1) cathode/anode combinations showed a clear hysteresis in the charge and discharge voltage profiles at 2C (Figure S5a and b), although it was much more pronounced for the C5/A1 cell. While there are many possible causes for this,[49,50] including lithium concentration gradients, varying particle lithiation rates, mechanical stresses, and side reactions, this suggests that the internal resistance is much higher for certain cathode/anode combinations at high discharge rates.

Overall, the rate performance results demonstrate that changing both the active material particle *size* and *configuration* can significantly affect the high-rate performance of single-layer pouch cells. It should be noted that the active material powders used here each contained a

distribution of particle sizes. Sieving each of them to obtain a more uniform particle size before electrode fabrication may further enhance these observed performance differences. Likewise, increasing the size difference between the small and large particles (to more than the two-fold difference used here), or further optimizing the architecture may produce even greater improvements.

3.3 Correlation of Pore Size Distribution to Performance

Mercury porosimetry was performed on all five calendered cathodes and anodes in order to gain further insight into the nature of the pore structure within these electrodes. The pore size distribution results revealed the presence of multiple peaks at different pore sizes for each cathode and anode (Figure 7a and 7c). The single-layer small particle cathode (C1; blue), which showed good rate performance results, had more pores between 1-2 µm compared to the other four cathodes, which all had fairly similar distributions comprising larger pores around 1

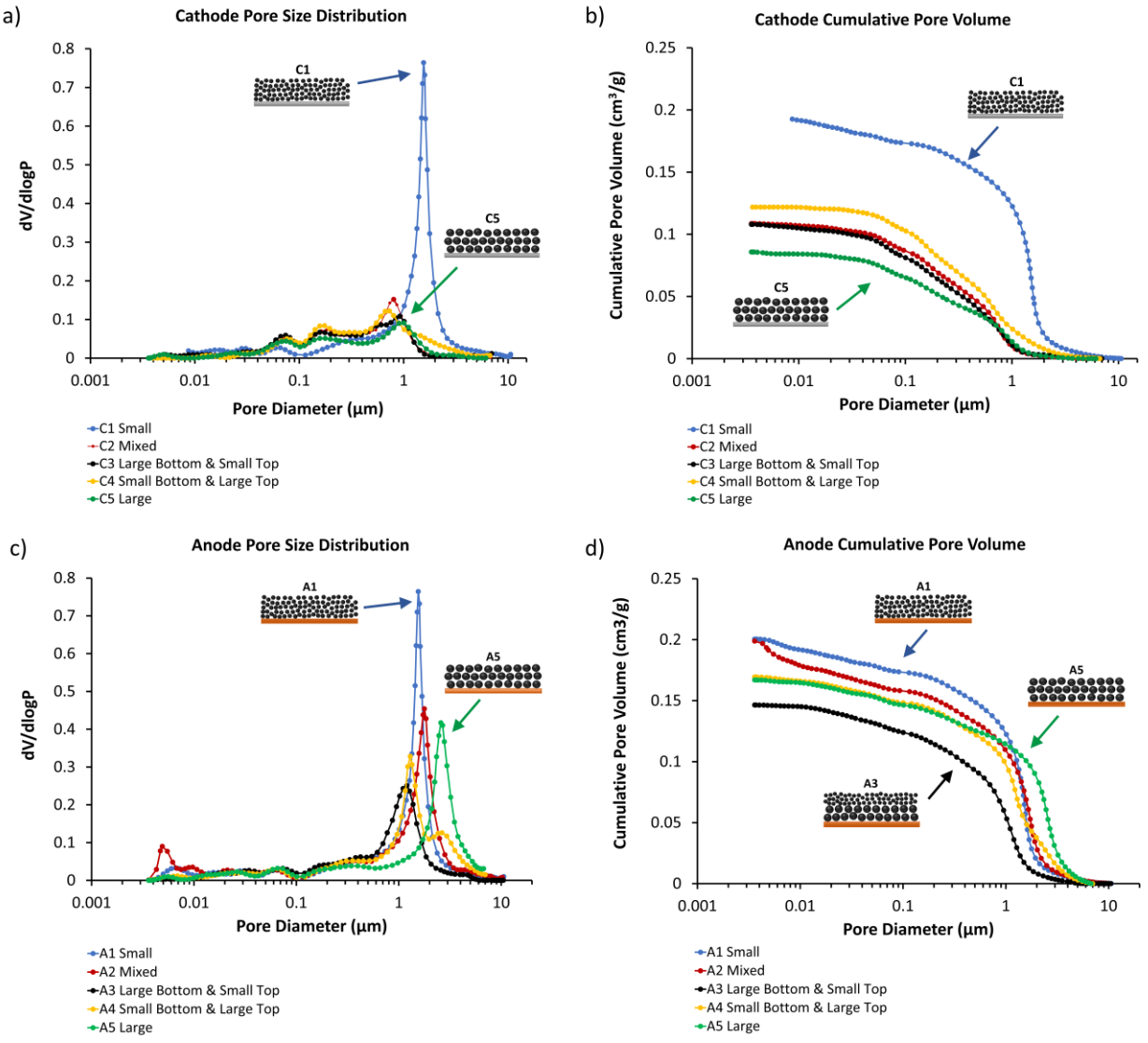

Figure 7. Pore size distribution (a and c) and cumulative pore volume (b and d) of all cathodes (a and b) and anodes (c and d) determined by mercury porosimetry. All electrodes were calendered to ~35% porosity.

μm and smaller pores around 75, 180, and 350 nm. Although the small particle cathode (C1) also had some pores around 350 nm, it had a different pore size distribution, with pores around 28 and 65 nm as well. It is important to point out that volume intrusion techniques such as mercury porosimetry do not give information about the tortuosity of the pores, just the quantitative volume at a corresponding size. Therefore, even though the small particle cathode (C1) had many large pores relative to the other cathode configurations, it is likely that these pores are also highly tortuous due to the smaller particle size and associated configuration, which would offset expected mass transport improvements based on the larger pore size alone.

In general, the pores in the anodes were slightly larger than those in the cathodes, with the biggest ones ranging from ~1-4 μm, which may be due to the relatively larger particle sizes used in the anodes. All the anodes also showed smaller pores around 65 and 300 nm. Interestingly, the single-layer large particle anode (A5; green), which showed good rate performance, contained more of the large pores (2-4 μm) compared to the other anodes, similar to the small particle cathode (C1). In addition, the two-layer anode with small particles near the current collector (A4; yellow), which also demonstrated good rate performance and was part of the best-performing cell, was the only anode with a clear bimodal distribution of large pores, with a peak at ~2.6 μm (the same peak seen in A5) and another one at ~1.3 μm (similar to the largest pores of all the other anodes), which could explain its superior performance. These results seem to suggest that a higher quantity of *large* pores results in better rate performance for both the cathodes and anodes, likely due to corresponding improved Li^+ diffusion.

Additional information can be gleaned from a plot of the total *cumulative* pore volume vs. pore diameter for each electrode (Figure 7b and 7d). Comparing just the single-layer cathodes, the small particle cathode (C1; blue) had the highest cumulative pore volume, while the large particle cathode (C5; green) had the lowest, and the mixed particle cathode (C2; red) had a cumulative pore volume in between. These results match the rate performance results for these three cathodes and suggest that a higher overall pore volume leads to better rate performance, likely due to better liquid-phase Li^+ diffusion. However, the results for the two-

layer cathodes were less clear, as the configuration with large particles near the current collector (C3; black) showed a lower cumulative pore volume than the opposite configuration (C4; yellow), even though it demonstrated better rate performance, indicating that the *distribution* or shape of the pores (rather than just the total pore volume) may also be important. Since both two-layer electrodes contain a layer of large particles and a layer of small particles, they should theoretically have similar total pore volumes. The observed differences between them could be due to differences in packing density when the large particle layer is coated on top of the small particle layer versus the opposite, or the creation of an interfacial zone between the two layers that has its own discrete packing density and pore size. It should be noted, though, that interfacial zones were not observable in the SEM cross-sections in Figure 2.

The differences between the total cumulative pore volume in the five anodes were less pronounced. However, some of the same trends were still observed. For example, the small particle anode (A1; blue) also showed the highest cumulative pore volume, while the large particle anode (A5; green) exhibited lower cumulative pore volume, and the mixed particle anode (A2; red) fell in between. As was the case for the two-layer cathodes, the two-layer anode with the large particles near the current collector (A3; black) had a lower cumulative pore volume than the two-layer anode with the small particles near the current collector (A4; yellow). Notably, the two best-performing anodes (large particle A5; green and two-layer A4 anode with the small particles near the current collector; yellow) had a higher percentage of larger pores, but did not have the highest cumulative pore volume, again highlighting the importance of pore size distribution. For the anode, a larger cumulative pore volume may be detrimental due to greater Li^+ loss from SEI formation over a larger surface area. However, it is challenging to correlate these results with the observed rate performance since the anode performance was highly dependent on which cathode it was paired with and is further complicated by factors such as orientation-specific Li^+ intercalation in graphite and the presence of an SEI layer.

More detailed characterization of the pore size distributions and mathematical modeling are needed to fully explain the rate performance results. However, overall the pore size measurements in conjunction with the rate capability data suggest that the distribution, location, and shape of the pores (not just the overall pore volume) may play an important role in determining performance.

3.4 Effect of Particle Size and Electrode Architecture on Long-Term Cycle Life

The effect of particle size and electrode architecture on cycle life was also explored, since characteristics that are beneficial for rate performance may not be beneficial for cycle life. A smaller number of cathode/anode combinations were selected for long-term cycling at two different discharge rates (C/2 and 2C) based on the rate performance results. The charge rate was kept constant at C/2 in both cases. These included a complete set of all five cathodes paired with the same best-performing large particle anode (A5), all four baseline cells, the best- and worst-performing cells from the rate capability tests (C3/A4 and C5/A1), several cells made with the two best cathodes (C3 and C1), one made with a medium-performing cathode (C2), and one made with the worst-performing two-layer cathode (C4) to cover a range of expected outcomes. Figure 9 shows the capacity fade for each of these thirteen combinations over 1000 cycles, with each data point representing an average of three to six cells. The small periodic interruptions in the data are due to resistance (HPPC) measurements taken every 100 cycles.

At a cycling rate of 2C, the capacity retention was somewhat low for all cells, with none achieving higher than 40%. This could be partially due to the higher charging rate used in these experiments (C/2) compared to the rate performance experiments (C/5). Comparing only the cells made with different cathodes but the same A5 anode (Figure 8a) reveals that the small particle cathode (C1; purple line) and the mixed particle cathode (C2; dark red line) performed the best, maintaining 29 mAh/g capacity (~30% retention) after 1000 cycles, while the large particle cathode (C5; black line) performed the worst (16 mAh/g; ~23% retention), which matches the rate performance results, except that the mixed particle cathode (C2) performed better in the cycle life test. Examining the complete data set (Figure 8a), there were seven

combinations that produced similar results (29 to 35 mAh/g; ~29-37% retention), including the best *rate* performance combination (two-layer C3 with large particles near the current collector/two-layer A4 with small particles near the current collector; 30 mAh/g; ~29% retention). The two best-performing cells were the C1 and C2 cathodes paired with the A4 anode (34 and 35 mAh/g and ~ 33% , respectively). The area specific impedance (ASI) values calculated from HPPC before cycling, after 500 cycles, and after 1000 cycles are plotted in Figure S1b. A comparison of the best (C2/A4) and worst (C5/A5) cells shows very little difference between the two, with a 1.5X increase in ASI after 1000 cycles for both combinations (from ~25 Ohm·cm^2 before cycling to ~39 Ohm·cm^2 after cycling; at 3.5V). These results suggest that even the best-performing electrode designs still suffer from capacity fade during long-term cycling at high C rates. Further optimization will be needed to improve this behavior.

On the other hand, the cells cycled at the slower discharge rate (C/2) displayed excellent performance despite their high areal capacities (Figure 8b). The best cathode/anode combinations were the small particle cathode (C1) paired with the mixed particle anode (A2) or the two-layer anode with small particles near the current collector (A4), and the mixed particle cathode (C2) paired with the same A4 anode, which all showed capacities between 127 and 129 mAh/g after 1000 cycles (80-82% retention). Conversely, the worst cathode/anode combination was the same small particle cathode (C1) paired with the small particle anode (A1), which had a capacity of only 22 mAh/g (17% retention). Since one of the best pairs and the worst pair both contained the same small particle cathode (C1), the improvement must be due to the different anode, suggesting that the particle size and structure of the *anode* makes a significant difference in the long-term cycling stability. The C3/A4 combination, which demonstrated the best rate performance, also performed well during C/2 cycling (120 mAh/g; 78% retention). A comparison of the ASI for the best (C1/A2) and worst (C1/A1) cells reveals a significant difference between the two (Figure S1a), with the C1/A1 combination showing a 6X increase in ASI after 1000 cycles (27 Ohm·cm^2 before cycling to 163 Ohm·cm^2 after cycling; at 3.5V), compared to just a 2X increase for the C1/A2 combination (27 Ohm·cm^2 before cycling to 53 Ohm·cm^2 after cycling; at 3.5V). This large increase in cell resistance is reflected in the

significantly larger charge-discharge voltage hysteresis (Figure S5c and d) and substantially faster capacity fade observed for the C1/A1 combination after repeated cycling. SEM cross-sections of the electrodes from these two cell combinations (Figures S3 and S4) did not reveal any obvious changes in electrode morphology after cycling, although some delamination of the anodes from the copper current collector was observed during post-mortem handling.

Table 1 compares the rate performance results with the cycle life results at both 2C and C/2 discharge rates, showing that while some cathode/anode combinations performed similarly across the board, others fared better under particular testing conditions. This suggests that some of the factors that affect rate performance differ from those that affect cycling performance. Additional experiments and further electrode optimization could produce better designs that improve *both* the rate performance and cycling performance of thick electrodes at high rates.

a)

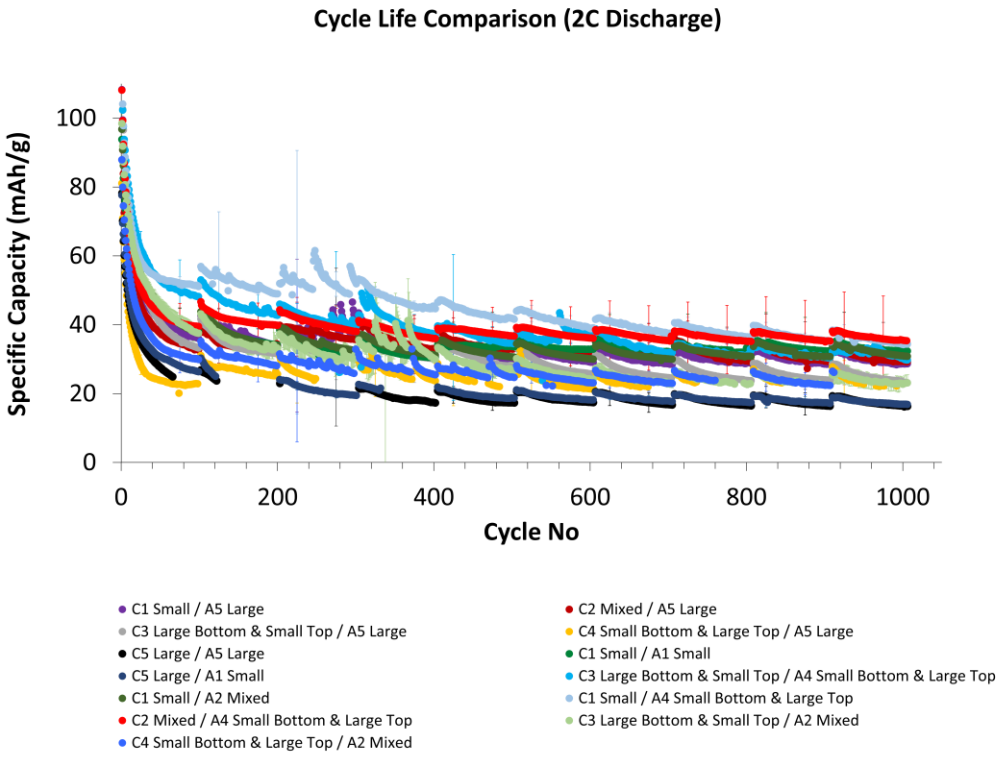
Cycle Life Comparison (2C Discharge)
Specific Capacity (mAh/g)
0
20
40
60
80
100
0
200
400
600
800
1000
Cycle No
C1 Small / A5 Large
C2 Mixed / A5 Large
C3 Large Bottom & Small Top / A5 Large
C4 Small Bottom & Large Top / A5 Large
C5 Large / A5 Large
C1 Small / A1 Small
C5 Large / A1 Small
C3 Large Bottom & Small Top / A4 Small Bottom & Large Top
C1 Small / A2 Mixed
C1 Small / A4 Small Bottom & Large Top
C2 Mixed / A4 Small Bottom & Large Top
C3 Large Bottom & Small Top / A2 Mixed
C4 Small Bottom & Large Top / A2 Mixed

b)

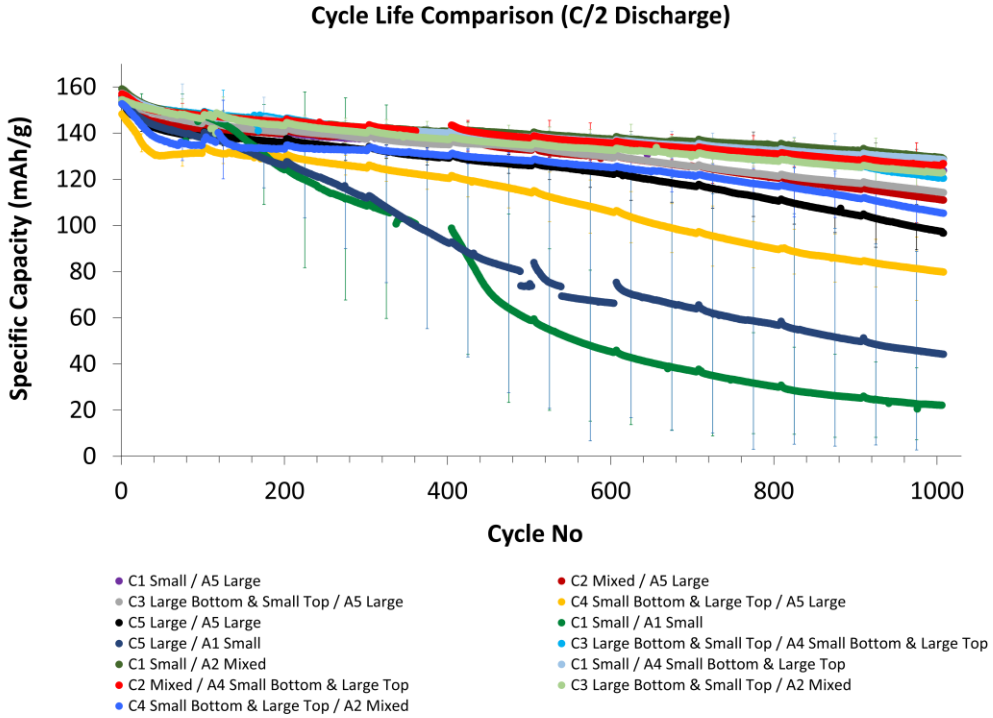
Cycle Life Comparison (C/2 Discharge)
Specific Capacity (mAh/g)
0
20
40
60
80
100
120
140
160
0
200
400
600
800
1000
Cycle No
C1 Small / A5 Large
C2 Mixed / A5 Large
C3 Large Bottom & Small Top / A5 Large
C4 Small Bottom & Large Top / A5 Large
C5 Large / A5 Large
C1 Small / A1 Small
C5 Large / A1 Small
C3 Large Bottom & Small Top / A4 Small Bottom & Large Top
C1 Small / A2 Mixed
C1 Small / A4 Small Bottom & Large Top
C2 Mixed / A4 Small Bottom & Large Top
C3 Large Bottom & Small Top / A2 Mixed
C4 Small Bottom & Large Top / A2 Mixed

Figure 8. Long-term cycle life comparison for single-layer pouch cells made with different cathode/anode combinations cycled at a) C/2 charge and 2C discharge and b) C/2 charge and discharge. Error bars represent the standard deviation of 3 to 6 cells for the C/2 discharge data and 3 cells for the 2C discharge data (averaged every 25 cycles). The systematic increases in capacity after every 100 cycles are due to HPPC tests at these points. The small breaks in some of the C/2 data are due to power outages that caused the cells to cycle without the data being recorded when the power returned. The small breaks in some of the 2C data are due to instrument testing fluctuations that occurred for some cells.

Table 1. Comparison of rate performance results (specific capacity and % rated capacity) and long-term cycling results (specific capacity and % capacity retention) after 1000 cycles at C/2 and 2C discharge rates for cells made with different cathode/anode combinations.

	Rate Performance at 2C			Long-Term Cycling at C/2 Discharge Rate (1000 Cycles)			Long-Term Cycling at 2C Discharge Rate (1000 Cycles)		
Cathode/Anode Combination	*Rank*	*Specific Capacity (mAh/g)*	*% of Rated Capacity*	*Rank*	*Specific Capacity (mAh/g)*	*% Capacity Retention*	*Rank*	*Specific Capacity (mAh/g)*	*% Capacity Retention*
C3 / A4	1	97	59	6	120	78	5	30	29
C1 / A5	2	91	55	4	124	79	7	29	29
C1 / A4	3	89	54	2	128	82	2	34	33
C3 / A3	4	88	53	N/A	N/A	N/A	N/A	N/A	N/A
C1 / A2	5	88	53	1	129	80	4	31	34
C3 / A2	6	87	53	5	123	80	10	23	25
C1 / A3	7	83	50	N/A	N/A	N/A	N/A	N/A	N/A
C3 / A1	8	78	47	N/A	N/A	N/A	N/A	N/A	N/A
C3 / A5	9	78	47	7	114	74	9	23	22
C2 / A4	10	76	46	3	127	81	1	35	33
C2 / A3	11	76	46	N/A	N/A	N/A	N/A	N/A	N/A
C2 / A2	12	71	43	N/A	N/A	N/A	N/A	N/A	N/A
C2 / A5	13	68	41	8	111	71	6	29	32
C4 / A4	14	68	41	N/A	N/A	N/A	N/A	N/A	N/A
C1 / A1	15	67	40	13	22	17	3	32	37
C2 / A1	16	63	38	N/A	N/A	N/A	N/A	N/A	N/A
C4 / A3	17	63	39	N/A	N/A	N/A	N/A	N/A	N/A
C4 / A1	18	58	35	N/A	N/A	N/A	N/A	N/A	N/A
C5 / A4	19	55	33	N/A	N/A	N/A	N/A	N/A	N/A
C5 / A3	20	53	32	N/A	N/A	N/A	N/A	N/A	N/A
C5 / A2	21	51	31	N/A	N/A	N/A	N/A	N/A	N/A
C4 / A2	22	50	30	9	105	69	8	26	25
C5 / A5	23	50	30	10	97	63	13	16	23
C4 / A5	24	46	28	11	80	54	11	22	28
C5 / A1	25	46	28	12	44	29	12	17	16

4. **Conclusions**

In conclusion, we evaluated 5 different thick electrode designs (3 single-layer and 2 two-layer) to determine how active material particle size and configuration affect high-rate performance and long-term cycle life in single-layer pouch cells. We found that simply decreasing the cathode active material secondary particle size from 12 µm to 6 µm led to a 1.8X capacity improvement at a discharge rate of 2C (from 50 to 91 mAh/g; 30% to 55% of rated capacity), likely due to better active material utilization as a result of the higher particle surface area. The six best-performing cells out of all 25 cathode/anode combinations all contained either the single-layer small particle cathode (C1) or the two-layer cathode with large particles near the current collector (C3), while the six worst-performing cells all contained cathodes with the opposite configurations (either the single-layer large particle cathode (C5) or the two-layer cathode with small particles near the current collector (C4)). Although the anodes did not show a clear trend, we found that anode design still plays an integral role in overall performance. For example, changing the configuration from a single-layer electrode to a two-layer electrode (with either a layer of large particles near the current collector and a layer of small particles on top or vice versa) did not significantly improve the performance when either the anode or cathode was changed individually. However, the *combination* of the two-layer cathode with large particles near the current collector (C3) and the two-layer anode with small particles near the current collector (A4) resulted in the best performance of all 25 cell designs, reaching 97 mAh/g at 2C (59% of rated capacity) and showing a 2X improvement over the worst-performing cathode/anode combination. These results highlight the importance of optimizing *both* the cathode and anode together.

Mercury porosimetry of the different electrode designs showed differences in pore size distributions, with most of the best-performing electrodes (small particle C1 cathode, large particle A5 anode, and two-layer A4 anode with small particles near the current collector) showing a higher percentage of larger pores. However, the two-layer C3 cathode did not contain a high percentage of large pores, and yet it was also one of the best-performing cathodes, indicating that in addition to the pore size, the pore *distribution* also plays a role.

Long-term cycling at a discharge rate of C/2 revealed significant differences in capacity retention depending on the electrode design, with the best combination (single-layer small particle C1 cathode with the single-layer mixed particle A2 anode or the two-layer A4 anode with small particles near the current collector) retaining 128-129 mAh/g (80-82% of the initial capacity) after 1000 cycles, and several others reaching > 120 mAh/g. While long-term cycling at 2C caused significant capacity fade in all cells, some electrode designs fared better than others, and additional design tailoring could improve these results. Changing the active material particle size and configuration are simple, straightforward approaches for improving transport in thick electrodes that are inexpensive, scalable, and easy to implement in current manufacturing processes. Further optimization of both the particle size and architecture should lead to more complete active material utilization in thick electrodes and better high-power performance for high energy density Li-ion batteries.

Conflicts of Interest

There are no conflicts to declare.

Acknowledgements

This research at Oak Ridge National Laboratory, managed by UT Battelle, LLC, for the U.S. Department of Energy (DOE) under contract DE-AC05-00OR22725, was sponsored by the Office of Energy Efficiency and Renewable Energy (EERE) Advanced Manufacturing Office (AMO) (Program Managers: David Hardy and Brian Valentine; Program Director Valri Lightner). We would like to thank Sergiy Kalnaus for his valuable discussions and input.

References

1 R. Schmuch, R. Wagner, G. Hörpel, T. Placke and M. Winter, *Nat. Energy*, 2018, **3**, 267–278.

2 S. Chen, F. Dai and M. Cai, *ACS Energy Lett.*, 2020, 3140–3151.

3 D. L. Wood, J. Li and C. Daniel, *J. Power Sources*, 2015, **275**, 234–242.

4 S. T. Myung, F. Maglia, K. J. Park, C. S. Yoon, P. Lamp, S. J. Kim and Y. K. Sun, *ACS Energy*

Lett., 2017, **2**, 196–223.

5 P. Li, H. Kim, S. Myung and Y. Sun, *Energy Storage Mater.*, 2021, **35**, 550–576.

6 Z. Zhang, Xin; Yang, Yongan, Zhou, *Chem. Soc. Rev.*, 2020, **49**, 3040–3071.

7 J. Li, Z. Du, R. E. Ruther, S. J. An, L. A. David, K. Hays, M. Wood, N. D. Phillip, Y. Sheng, C. Mao, S. Kalnaus, C. Daniel and D. L. Wood, *JOM*, 2017, **69**, 1484–1496.

8 Y. Kuang, C. Chen, D. Kirsch and L. Hu, *Adv. Energy Mater.*, 2019, 1901457.

9 N. Ogihara, Y. Itou, T. Sasaki and Y. Takeuchi, *J. Phys. Chem. C*, 2015, **119**, 4612–4619.

10 T. Danner, M. Singh, S. Hein, J. Kaiser, H. Hahn and A. Latz, *J. Power Sources*, 2016, **334**, 191–201.

11 Z. Du, D. L. Wood, C. Daniel, S. Kalnaus and J. Li, *J. Appl. Electrochem.*, 2017, **47**, 405–415.

12 J. St. John, 24M Unveils the Reinvented Lithium-Ion Battery, https://www.greentechmedia.com/articles/read/24m-unveils-the-reinvented-lithium-ion-battery.

13 H. Zheng, J. Li, X. Song, G. Liu and V. S. Battaglia, *Electrochim. Acta*, 2012, **71**, 258–265.

14 M. Singh, J. Kaiser and H. Hahn, *J. Electrochem. Soc.*, 2015, **162**, A1196–A1201.

15 M. Singh, J. Kaiser and H. Hahn, *JEAC*, 2016, **782**, 245–249.

16 K. G. Gallagher, S. E. Trask, C. Bauer, T. Woehrle, S. F. Lux, M. Tschech, P. Lamp, B. J. Polzin, S. Ha, B. Long, Q. Wu, W. Lu, D. W. Dees and A. N. Jansen, *J. Electrochem. Soc.*, 2016, **163**, A138–A149.

17 S. Golmon, K. Maute and M. L. Dunn, *Int. J. Numer. Methods Eng.*, 2012, **92**, 475–494.

18 S. Golmon, K. Maute and M. L. Dunn, *J. Power Sources*, 2014, **253**, 239–250.

19 C. Liu, Lin; Guan, Pengjian; Liu, *J. Electrochem. Soc.*, 2017, **164**, A3163–A3173.

20 Y. Qi, T. Jang, V. Ramadesigan, D. T. Schwartz and V. R. Subramanian, *J. Electrochem. Soc.*, 2017, **164**, A3196–A3207.

21 V. Dai, Yiling; Srinivasan, *J. Electrochem. Soc.*, 2016, **163**, A406–A416.

22 W. Mai, F. L. E. Usseglio-viretta, A. M. Colclasure and K. Smith, *Electrochim. Acta*, 2020, **341**, 136013.

23 C. L. Cobb and S. E. Solberg, *J. Electrochem. Soc.*, 2017, **164**, A1339–A1341.

24 F. L. E. Usseglio-viretta, W. Mai, A. M. Colclasure, M. Doeff, E. Yi and K. Smith,

Electrochim. Acta, 2020, **342**, 136034.

25 Y. Xu, M. Zhou and Y. Lei, *Adv. Energy Mater.*, 2016, **6**, 1–24.

26 J. S. Sander, R. M. Erb, L. Li, A. Gurijala and Y.-M. Chiang, *Nat. Energy*, 2016, **1**, 1–7.

27 A. R. Billaud, Juliette; Bouville, Florian; Magrini, Tommaso; Villevieille, Claire; Studart, *Nat. Energy*, 2016, **1**, 16097.

28 D. S. Ashby, C. S. Choi, M. A. Edwards, A. A. Talin, H. S. White and B. S. Dunn, *ACS Appl. Energy Mater.*, 2020, **3**, 8402–8409.

29 K. Mckelvey, A. A. Talin, B. Dunn and H. S. White, *J. Electrochem. Soc.*, 2017, **164**, A2500–A2503.

30 S. Behr, R. Amin, Y. Chiang and A. P. Tomsia, *Ceram. Forum Int.*, 2015, **92**, 39–43.

31 C. Huang, M. Dontigny, K. Zaghib and P. S. Grant, *J. Mater. Chem. A*, 2019, **7**, 21421–21431.

32 K. Chen, M. Ji, V. Goel, C. Yang, S. Kazemiabnavi, S. M. Mortuza, E. Kazyak, J. Mazumder, K. Thornton, J. Sakamoto and P. Dasgupta, *J. Power Sources*, 2020, **471**, 228475.

33 P. Smyrek, T. Bergfeldt and J. Hans, *J. Mater. Chem. A*, 2019, **7**, 5656–5665.

34 P. Pfleging, Wilhelm; Gotcu, *Appl. Sci.*, 2019, **9**, 3588.

35 C. J. Bae, C. K. Erdonmez, J. W. Halloran and Y. M. Chiang, *Adv. Mater.*, 2013, **25**, 1254–1258.

36 C. Sun, S. Liu, X. Shi, C. Lai, J. Liang and Y. Chen, *Chem. Eng. J.*, 2020, **381**, 122641.

37 Y. Pang, Y. Cao, Y. Chu, M. Liu, K. Snyder and D. Mackenzie, *Adv. Funct. Mater.*, 2020, **30**, 1906244.

38 L. Xue, X. Li, Y. Liao and L. Xing, *J. Solid State Electrochem.*, 2015, **19**, 569–576.

39 J. F. Whitacre, K. Zaghib, W. C. West and B. V Ratnakumar, 2008, **177**, 528–536.

40 D. Liu, L. Chen, T. Liu, W. Chu and C. Tiu, 2017, 1235–1241.

41 R. Diehm, J. Kumberg, C. Dörrer, M. Müller, W. Bauer, P. Scharfer and W. Schabel, 2020, **1901251**, 1–7.

42 L. Chen, D. Liu, T. Liu, C. Tiu, C. Yang, W. Chu and C. Wan, *J. Energy Storage*, 2016, **5**, 156–162.

43 Y. Chen, Z. Zhou, N. Li, S. Jiao and H. Chen, 2019, **323**, 1–9.

44 C. Huang, N. P. Young, J. Zhang, H. J. Snaith and P. S. Grant, *Nano Energy*, 2017, **31**, 377–385.

45 W. Du, A. Gupta, X. Zhang, A. Marie and W. Shyy, *Int. J. Heat Mass Transf.*, 2010, **53**, 3552–3561.

46 S. Jin, J. Li, C. Daniel, D. Mohanty, S. Nagpure and D. L. Wood, *Carbon N. Y.*, 2016, **105**, 52–76.

47 N. C. Gallego, C. I. Contescu, H. M. Meyer, J. Y. Howe, R. A. Meisner, E. A. Payzant, M. J. Lance, S. Y. Yoon, M. Denlinger and D. L. Wood, *Carbon N. Y.*, 2014, **72**, 393–401.

48 K. Persson, V. A. Sethuraman, L. J. Hardwick and Y. Hinuma, *J. Phys. Chem. Lett.*, 2010, **1**, 1176–1180.

49 B. Lu, Y. Song, Q. Zhang, J. Pan, Y. T. Cheng and J. Zhang, *Phys. Chem. Chem. Phys.*, 2016, **18**, 4721–4727.

50 V. J. Ovejas and A. Cuadras, *Sci. Rep.*, 2019, **9**, 1–9.